

Quantum supremacy in driven quantum many-body systems

Jirawat Tangpanitanon,^{1,*} Supanut Thanasilp,¹ Marc-Antoine Lemonde,¹ Ninnat Dangniam,^{2,3} and Dimitris G. Angelakis^{1,4,†}

¹*Centre for Quantum Technologies, National University of Singapore, 3 Science Drive 2, Singapore 117543*

²*Department of Physics and Center for Field Theory and Particle Physics, Fudan University, Shanghai 200433, China*

³*State Key Laboratory of Surface Physics, Fudan University, Shanghai 200433, China*

⁴*School of Electrical and Computer Engineering,
Technical University of Crete, Chania, Greece 73100*

(Dated: March 27, 2022)

A crucial milestone in the field of quantum simulation and computation is to demonstrate that a quantum device can perform certain tasks that are impossible to reproduce by a classical computer with any reasonable resources. Such a demonstration is referred to as quantum supremacy. One of the most important questions is to identify setups that exhibit quantum supremacy and can be implemented with current quantum technology. The two standard candidates are boson sampling and random quantum circuits. Here, we show that quantum supremacy can be obtained in generic periodically-driven quantum many-body systems. Our analysis is based on the eigenstate thermalization hypothesis and strongly-held conjectures in complexity theory. To illustrate our work, we give examples of simple disordered Ising chains driven by global magnetic fields and Bose-Hubbard chains with modulated hoppings. Our proposal opens the way for a large class of quantum platforms to demonstrate and benchmark quantum supremacy.

I. INTRODUCTION

Quantum computational supremacy is the ability of quantum devices to efficiently perform certain tasks that cannot be efficiently simulated on a classical computer [1, 2]. Early proposals for realizing quantum supremacy include boson sampling [3–5] and random quantum circuits [6–8]. In both cases, the computational hardness stems from the inability of a classical computer to efficiently sample the output probabilities of a complex quantum evolution. Experimental efforts towards achieving quantum supremacy include optical networks for boson sampling [9–13] and superconducting circuits for random circuits [14]. Signatures of quantum supremacy have been observed recently with 53 superconducting qubits [15].

Analog quantum simulators are controllable quantum platforms specifically built to implement complex quantum many body models [16–19]. In these experiments, complex quantum dynamics have been implemented which cannot be reproduced with existing classical numerics and have shed light to important questions in quantum matter [20]. However, rigorous proof of quantum supremacy involving complexity theory in those systems has not been so far possible, with the exceptions of the 2D quantum Ising [21, 22] and the 2D cluster-state models [23].

In this work, we provide evidence that when generic isolated periodically-driven quantum many-body systems thermalize, in the sense that any observables can be obtained from the microcanonical ensemble, their output

distribution cannot be efficiently simulated on a classical computer. These constitute a large class of quantum simulators that are currently available [14, 24–26]. Our results are built on the Eigenstate Thermalization Hypothesis (ETH) and strongly-held conjectures in the complexity theory. We support our findings by examining specific examples of disordered quantum Ising chains driven by a global magnetic field and the Bose-Hubbard chain with modulated hoppings. These models have been widely implemented in the experiments [14, 25–28] and make our work of broad interest to the experimental community.

II. RESULTS

General framework.— Let us consider a generic periodically-driven quantum many-body system whose Hamiltonian is described by $\hat{H}(t) = \hat{H}_0 + f(t)\hat{V}$, where \hat{H}_0 is the undriven Hamiltonian, \hat{V} is the driving Hamiltonian such that $[\hat{H}_0, \hat{V}] \neq 0$, and $f(t)$ is periodic with the period T . We require that the time-averaged Hamiltonian $\hat{H}_{\text{ave}} = \frac{1}{T} \int_0^T \hat{H}(t) dt$ is many-body, in the sense that its eigenenergies cannot be written as a linear combination of single-particle energies [29].

Let $\mathcal{Z} = \{|\mathbf{z}\rangle = \otimes_i^L |z_i\rangle\}$ be a complete basis of many-body Fock states, where $z_i = \{0, 1, 2, \dots, D_i - 1\}$ denotes the local state with the local dimension D_i and the number of sites L . We assume here without loss of generality that $D_i = D$ for $\forall i \in [1, L]$. The dimension of the Hilbert space is $N = D^L$. The state after M driving periods is $|\psi_M\rangle = \hat{U}_F^M |\mathbf{z}_0\rangle$, where $\hat{U}_F = \hat{T} \exp\left(-i \int_0^T \hat{H}(t) dt\right) \equiv \exp\left(-i \hat{H}_F T\right)$, \hat{T} is the time-ordering operator. We assume that the initial state $|\mathbf{z}_0\rangle$ is a product state.

* cqtjt@nus.edu.sg

† dimitris.angelakis@qubit.org

The effective time-independent Floquet Hamiltonian \hat{H}_F fully describes the dynamics probed at stroboscopic times $t = nT$. The probability of measuring the Fock state \mathbf{z} is then $p_M(\mathbf{z}) = |\langle \mathbf{z} | \psi_M \rangle|^2$ with

$$\langle \mathbf{z} | \psi_M \rangle = \sum_{\mathbf{z}_1, \dots, \mathbf{z}_{M-1} \in \mathcal{Z}} \prod_{m=0}^{M-1} \langle \mathbf{z}_{m+1} | \hat{U}_F | \mathbf{z}_m \rangle, \quad (1)$$

where the sum is performed over $M - 1$ complete sets of basis states. More precisely, the set of basis states $\{\mathbf{z}_m\}$ is associated with the quantum evolution after m driving cycles with \mathbf{z}_0 ($\mathbf{z}_M = \mathbf{z}$) being the initial (readout) configuration. The expression in Eq. (1) can be viewed as the Feynman's path integral where each trajectory is defined by a set of basis states $\{\mathbf{z}_0, \mathbf{z}_1, \dots, \mathbf{z}_M\}$.

The ETH states that isolated many-body quantum systems without symmetry thermalize by their own dynamics after a long enough time, regardless of their initial state. In that case, any generic observable is expected to evolve toward the micro-canonical ensemble predictions associated with the energy $\bar{E} \pm \Delta E$, where $\bar{E} = \langle \mathbf{z}_0 | \hat{H}_F | \mathbf{z}_0 \rangle$ and ΔE is the corresponding variance. In the thermodynamic limit, this ensemble is equivalent to the canonical ensemble with a temperature $\hbar \bar{E} / k_B$ [30]. For driven quantum many-body systems, it has been shown that not only thermalization still occurs, but that for low-frequency driving, the associated temperature becomes infinite [31]. In this limit, the Floquet operator \hat{U}_F can be thought of as an instance from the Circular Orthogonal Ensemble (COE). This is an ensemble of matrices whose elements are independent normal complex random variables subjected to the orthogonality and the unitary constraints. This emergent randomness is the particular ingredient responsible for the hardness in calculating the output probability of Eq. (1), as there are exponentially many random Feynman trajectories that are equally important.

Outline of the proof for quantum supremacy.— To understand the computational task, let us first define some essential terms used in the complexity theory, namely *approximating*, *sampling*, *multiplicative error* and *additive error*. Imagine an analog quantum device built to mimic quantum dynamics characterized by $p_M(\mathbf{z}) = |\langle \mathbf{z} | \psi_M \rangle|^2$. In practice, such device will produce output probabilities $q(\mathbf{z})$ that differ from $p_M(\mathbf{z})$ due to noise, decoherence and imperfect control. Both probabilities are said to be multiplicatively close if

$$|p_M(\mathbf{z}) - q(\mathbf{z})| \leq \alpha p_M(\mathbf{z}) \quad (2)$$

where $\alpha \geq 0$. The task of *approximating* $p_M(\mathbf{z})$ up to *multiplicative error* is to calculate $q(\mathbf{z})$ that satisfies the above equation for a given \mathbf{z} . However, multiplicative error is difficult to achieve in the experiments as the allowed error is proportional to $p_M(\mathbf{z})$ which can be much smaller than unity. A more feasible one is additive error defined as

$$\sum_{\mathbf{z} \in \mathcal{Z}} |p_M(\mathbf{z}) - q(\mathbf{z})| \leq \beta, \quad (3)$$

with $\beta > 0$. Note that the additive error involves all possible output strings $\mathbf{z} \in \mathcal{Z}$, while the multiplicative one is defined for each \mathbf{z} .

The task of approximating $p_M(\mathbf{z})$ even with additive error is still unrealistic as it requires the number of measurements that grows exponentially with the size of the systems. What a quantum device can do is to sample strings from $q(\mathbf{z})$. Hence, we define the task of *sampling from* $p_M(\mathbf{z})$ up to *additive error* as generating strings from $q(\mathbf{z})$, while $q(\mathbf{z})$ is additively close to $p_M(\mathbf{z})$. This task is our central task to show quantum supremacy and is exactly what we mean by simulation. Note that the task itself is different from ‘certification of quantum supremacy’ [32] which is to certify if Eq. (3) holds.

To show that the above sampling task cannot be done efficiently by a classical computer, we follow the standard argument which proceeds as follows. Suppose that there is a classical machine \mathcal{C} that can *sample from* $p_M(\mathbf{z})$ up to *additive error* and that the distribution of $p_M(\mathbf{z})$ anti-concentrates, i.e.

$$\Pr \left(p_M(\mathbf{z}) > \frac{\delta}{N} \right) \geq \gamma, \quad (4)$$

for some positive constants $\delta, \gamma > 0$ for all $\mathbf{z} \in \mathcal{Z}$ [33]. Here, the distribution is obtained from a set of unitary matrices $\{\hat{U}_F\}$ that are realizable in an experiment. The Stockmeyer theorem states that, with the help of an NP oracle, the machine \mathcal{C} can also *approximate* $p_M(\mathbf{z})$ up to *multiplicative error* for some outcomes \mathbf{z} , given that $p_M(\mathbf{z})$ anticenters [34]. Notice that the sampling task is converted to the approximation task in this step. If the latter is #P-hard, then a machine \mathcal{C} would imply the collapse of the polynomial hierarchy (PH) to the third level, which is strongly believed to be unlikely in computer science. Hence, assuming that the PH does not collapse, we reach the conclusion that a classical machine \mathcal{C} cannot exist.

To validate the above arguments, it is crucial to discuss how likely that those #P-hard instances can be realized in the experiment. Let us define the notions of *worst-case* and *average-case* hardness. In the experiment, a set of output probabilities will be obtained from many unitary matrices and output strings. The worst-case is when there is at least one instance in the set that is hard to approximate with multiplicative error. However, that one instance may be impractical to find in the experiments. More desirable is average-case hardness where most instances are hard.

In what follows, we provide evidence for quantum supremacy in analog quantum systems. We begin by proving the following theorems for the COE.

Theorem 1 *Let \mathcal{Y} be a set of output probabilities $\tilde{p}_M(\mathbf{z}) = |\langle \mathbf{z} | \hat{U}_{\text{COE}}^M | \mathbf{z}_0 \rangle|^2$ obtained from all possible COE matrices $\{\hat{U}_{\text{COE}}\}$ and all possible output strings $\mathbf{z} \in \mathcal{Z}$. Approximating $\tilde{p}_M(\mathbf{z})$ in \mathcal{Y} up to multiplicative error is #P hard in the worst case.*

Theorem 2 *The distribution of $\tilde{p}_M(\mathbf{z})$ in \mathcal{Y} anticoncentrates with $\delta = 1$ and $\gamma = 1/e$, where e is the base of the natural logarithm.*

Here, we use $\hat{U}_{\text{COE}}(\tilde{p}_M(\mathbf{z}))$ instead of $\hat{U}_F(p_M(\mathbf{z}))$ to stress the fact that even though ETH implies that \hat{U}_F is an instance drawn from the COE, not all COE matrices will be realized by $\{\hat{U}_F\}$. To ensure that the hard instance in \mathcal{Y} can be found within $\{\hat{U}_F\}$, we further assume two conjectures to arrive at quantum supremacy for our analog quantum systems.

Conjecture 1 (Average-case hardness) *For any $1/2e$ fraction of \mathcal{Y} , approximating $\tilde{p}_M(\mathbf{z})$ up to multiplicative error with $\alpha = 1/4 + o(1)$, where $o(\cdot)$ is little-o notation[35], is as hard as the hardest instance.*

Conjecture 2 (Computational ETH) *Let η be the fraction of matrices $\{\hat{U}_{\text{COE}}\}$ that anti-concentrates but do not correspond to any unitary matrices in the experimentally accessible set $\{\hat{U}_F\}$. Then $\eta = 1/4e$.*

Informally, Conjecture 1 assumes the worst-to-average case reduction in \mathcal{Y} which is common in most quantum supremacy proposals [36]. Conjecture 2 connects the mathematically constructed COE with physical analog quantum systems, by stating that most instances in $\{\hat{U}_{\text{COE}}\}$ can be realized with $\{\hat{U}_F\}$. The fractions used in Conjecture 1 and 2 are chosen to ensure that some hard instances in \mathcal{Y} can be realized with $\{\hat{U}_F\}$.

Now, we state the main theorem of this work. The proof, provided in Method IV A, can be derived using the standard Stockmeyer theorem.

Theorem 3 *Assuming Conjecture 1 and 2, the ability to classically sample from $p_M(\mathbf{z})$ up to an additive error $\beta = 1/2e$ for all unitary matrices in $\{\hat{U}_F\}$ implies the collapse of the polynomial hierarchy to the third level.*

We note that, comparing to existing quantum supremacy proposals, the reliance of Theorem 3 on Conjecture 2 is not standard and may be seen as undesirable. But in our viewpoint, this theorem makes a connection between computational complexity and strongly-held physical conjecture that is applicable to a broad class of generic periodically-driven quantum systems. Proving or disproving Conjecture 2, either directly or indirectly by refutation of Theorem 3 while Conjecture 1 holds true, is by itself of fundamental interest in physics.

#P hardness of simulating COE quantum dynamics. To prove Theorem 1, we first notice that the COE is an ensemble of all orthogonal unitary matrices. This includes the well-known instantaneous quantum polynomial (IQP) circuits [6] which take the form $\hat{U}_{\text{IQP}} = \hat{\mathcal{H}}\hat{\mathcal{Z}}^M\hat{\mathcal{H}}$, where $\hat{\mathcal{H}}$ consists of Hadamard gates and $\hat{\mathcal{Z}}$ is an arbitrary (possibly non-local) diagonal gate on the computational basis, both acting on all qubits. The IQP circuits constitute one of the early proposals of quantum supremacy. Multiplicative approximation of their output probabilities are known to be #P hard in the worst

case [37, Theorem 1.4]. Since $\hat{U}_{\text{IQP}}^M = \hat{\mathcal{H}}\hat{\mathcal{Z}}^M\hat{\mathcal{H}}$ and the elements of $\hat{\mathcal{Z}}^M$ can be redefined to give a general form of the IQP circuits, we conclude that there exists at least one instance in \mathcal{Y} that is #P hard for multiplicative approximation.

To see how the hardness could emerge for a typical instances in \mathcal{Y} (Conjecture 1), we map the path integral in Eq. (1) to the partition function of a classical Ising model with random complex fields. The latter is widely conjectured to be #P-hard on average for multiplicative approximation [21, 38]. The protocol is twofold: first we map the COE unitary evolution on *universal* random quantum circuits and second we derive a complex Ising model from those circuits following Ref. [7].

By definition, a COE unitary evolution can be written as $\hat{U}_{\text{COE}} = \hat{U}_{\text{CUE}}^T \hat{U}_{\text{CUE}}$ where \hat{U}_{CUE} is a random matrix drawn from the Circular Unitary Ensemble (CUE). The latter is the ensemble of Haar-random matrices [39]. Mathematically, \hat{U}_{CUE} can be efficiently decomposed into a set of universal quantum gates [7]. Following Ref. [7], we choose random quantum circuits consisting of $n + 1$ layers of gates and $\log_2 N$ qubits, as shown in Fig. 1(a). The first layer consists of Hadamard gates applied to all qubits. The following layers consist of randomly chosen single-qubit gates from the set $\{\sqrt{\hat{X}}, \sqrt{\hat{Y}}, \hat{T}\}$ and two-qubit controlled-Z (CZ) gates. Here, $\sqrt{\hat{X}}$ ($\sqrt{\hat{Y}}$) represents a $\pi/2$ rotation around the \hat{X} (\hat{Y}) axis of the Bloch sphere and \hat{T} is a non-Clifford gate representing a diagonal matrix $\{1, e^{i\pi/4}\}$. Such circuits have been shown to be approximately t -design [40] for an arbitrary large t when $n \rightarrow \infty$, which implies the CUE evolution [41]. The operator \hat{U}_{CUE}^T can be implemented by reversing the order of the gates in \hat{U}_{CUE} and replacing $\sqrt{\hat{Y}}$ with $\sqrt{\hat{Y}}^T$.

The mathematical procedure to map random quantum circuits to classical complex Ising models is provided in Ref. [7]. Specifically, $\tilde{p}_M(\mathbf{z})$ from the circuit $(\hat{U}_{\text{CUE}}^T \hat{U}_{\text{CUE}})^M$, as depicted in Fig. 1(a), can be calculated from the partition function,

$$\langle \mathbf{z} | \hat{U}_{\text{COE}}^M | \mathbf{z}_0 \rangle = \sum_{\mathbf{s} \in \mathcal{S}} A(\mathbf{s}) \exp \left[\frac{i\pi}{4} \left(\sum_i h_i s_i + \sum_{\langle i,j \rangle} J_{ij} s_i s_j \right) \right]. \quad (5)$$

Here, $A(\mathbf{s})$ is the degeneracy number associated with a classical spin configuration \mathbf{s} in the lattice \mathcal{S} , $s_i = \pm 1$, h_i represents a on-site field on site i and J_{ij} represents the coupling between the classical spins on site i and j . The intuition behind the mapping is that the sum over all possible paths in Eq. (1) is translated into the sum over all possible classical spin configurations, where the phase accumulated in each path is given by the energy of the complex Ising lattice \mathcal{S} . To gain intuitive understanding of this standard mapping, we provide a diagrammatic approach to visualize the lattice \mathcal{S} and extract the field parameters $\{h_i\}$, $\{J_{ij}\}$. To begin with, we use the random circuit in Fig. 1(b) as a demonstration. The mathematical descriptions behind each steps are discussed in

(a) Periodically driven quantum many-body systems

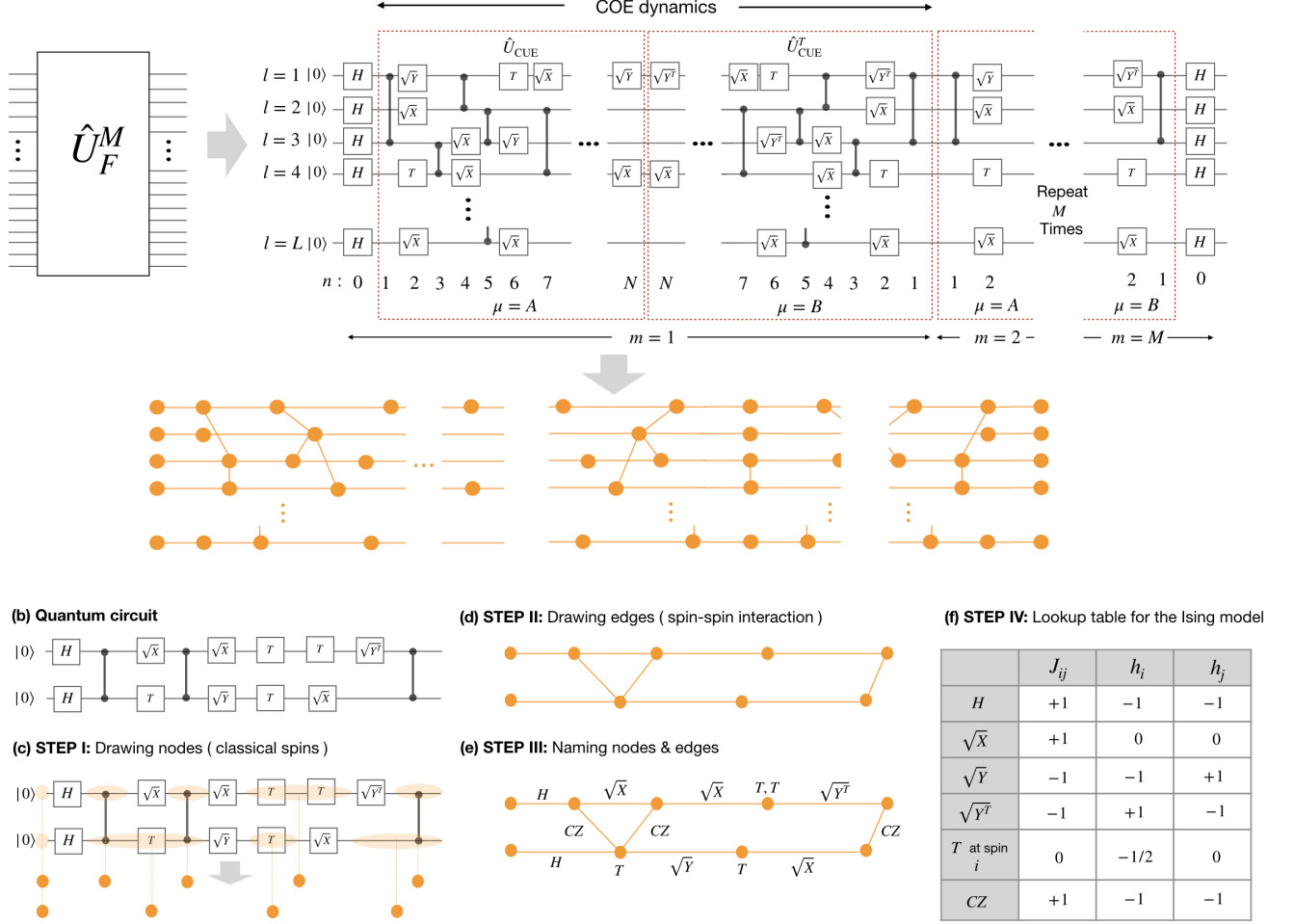


FIG. 1. **Mapping driven many-body dynamics to the partition function of complex Ising lattices:** (a) An example of a random circuit that generates COE dynamics and its conversion to the Ising model. (b) An example of a simple random quantum circuit, illustrating the mapping to the classical Ising model. STEP I to STEP III in the diagrammatic procedure are shown in (b)-(d), respectively. (e) Lookup table for the contribution of each gate to the local fields h_i , h_j and the interaction J_{ij} in the Ising lattice.

Methods.

- **STEP I** - For each qubit, draw a circle between every consecutive non-diagonal gates, see Fig. 1(c). Each circle or ‘node’ represents one classical spin.
- **STEP II** - For each qubit, draw a horizontal line between every consecutive nodes i, j , see Fig. 1(d). These lines or ‘edges’ represent interaction J_{ij} between two neighboring spins in the same row. In addition, draw a line between every two nodes that are connected by CZ gates. These lines represent the interaction J_{ij} between spins in different rows.
- **STEP III** - Labeling each nodes and edges with the corresponding gates, see Fig. 1(e).
- **STEP IV** - Use the lookup table in Fig. 1(f) to specify h_i and J_{ij} introduced by each gate. For

example, the \sqrt{Y} gate that acts between nodes i and j adds -1 to J_{ij} , -1 to h_i and $+1$ to h_j . We use the convention that the leftmost index represents the leftmost node. Also, the two T -gates that are enclosed by the node i will add $0.5 + 0.5 = +1$ to the local field h_i .

- **STEP V** - Finally, spins at the leftmost side of the lattice are fixed at $+1$, corresponding to the initial state $|0\rangle$. Similarly, spins at the rightmost side of the lattice are fixed according to the readout state $|\mathbf{z}\rangle$.

Following the above recipe, we provide the exact form of the parameters in the Ising model for the COE dynamics in Methods, showing that the field parameters $\{h_i\}$ and $\{J_{ij}\}$ are quasi-random numbers with no apparent structure. Specifically, neither the phase $\pi \sum_i h_i s_i / 4$

nor the phase $\pi \sum_{\langle i,j \rangle} J_{ij} s_i s_j / 4$ is restricted to the values $0, \pi/2, \pi, 3\pi/2 \pmod{2\pi}$ for each spin configurations \mathbf{s} . Without such stringent restrictions, approximating the partition function up to multiplicative error is known to be $\#P$ -hard in the worst case [37, Theorem 1.9]. This motivates a widely used conjecture in quantum supremacy proposals that such task is also hard on average [21, 38].

We note here the major differences between random quantum circuits as proposed in Ref. [7] and our systems. Firstly, our systems are analog with no physical quantum gates involved. The decomposition to quantum gates is only done mathematically. Secondly, our system has discrete time-reversal symmetry, while such symmetry is absent in random quantum circuits. Consequently, the COE in our system is achieved from the Floquet operator \hat{U}_F , while the CUE in random quantum circuits are achieved from the entire unitary evolution. In addition, \hat{U}_F^M in our system does not have the t -design property due to the COE [42, pp.117-119]. However, as shown above, the hardness arguments for the random quantum circuits can be naturally applied to our case.

Anti-concentration of COE dynamics.- To prove Theorem 2, we write

$$\langle \mathbf{z} | \hat{U}_{\text{COE}} | \mathbf{z}_0 \rangle = \sum_{\epsilon=0}^{N-1} d_{\epsilon}(\mathbf{z}) e^{i\phi_{M,\epsilon}}, \quad (6)$$

where $d_{\epsilon}(\mathbf{z}) = \langle \mathbf{z} | E_{\epsilon} \rangle \langle E_{\epsilon} | \mathbf{z}_0 \rangle$, $\phi_{M,\epsilon} = ME_{\epsilon}T \pmod{2\pi}$, $|E_{\epsilon}\rangle$ is an eigenstate of \hat{H}_F with eigenenergy E_{ϵ} . For COE operator, $d_{\epsilon}(\mathbf{z})$ are real [39] and their distribution, denoted as $\text{Pr}(d)$, is given by the Bessel function of the second kind as depicted in Fig. 2(a), see Methods. The latter implies that the values of $d_{\epsilon}(\mathbf{z})$ for different ϵ and \mathbf{z} do not concentrate on a particular value.

Now let us consider the statistics of the phases $\{\phi_{M,\epsilon}\}$. We define the level spacing as $r_{\epsilon} = \min(\delta_{\epsilon+1}, \delta_{\epsilon}) / \max(\delta_{\epsilon+1}, \delta_{\epsilon})$ with $\delta_{\epsilon} = \phi_{\epsilon+1} - \phi_{\epsilon} > 0$. For a single driving cycle $M = 1$, the phases $\{\phi_{1,\epsilon}\}$ for COE are known to exhibit phase repulsion, i.e. the phases are correlated [31]. The COE distribution $\text{Pr}_{\text{COE}}(r_{\epsilon})$ is depicted in 2(b), showing the peak around $r = 0.5$. For multiple driving cycles $M \gg 2\pi/E_{\epsilon}T$, the correlations are erased due to energy folding, i.e. the effect of the modulo 2π . This results in the Poisson (POI) distribution of the level spacing, $\text{Pr}_{\text{POI}}(r_{\epsilon}) = 2/(1+r_{\epsilon}^2)$, with the peak at $r = 0$, see Fig. 2(b).

The Bessel function distribution of $d_{\epsilon}(\mathbf{z})$ and the POI distribution of $\phi_{M,\epsilon}$ ensures that the output distribution $\text{Pr}(p)$ is not concentrated. Specially, $\text{Pr}(p)$ follows the so-called Porter-Thomas distribution $\text{Pr}_{\text{PT}}(p) = Ne^{-Np}$, which implies that the system explores the entire Hilbert space. This satisfies the anti-concentration condition since $\text{Pr}_{\text{PT}}(p > \frac{1}{N}) = \int_{Np=1}^{\infty} d(Np) e^{-Np} = 1/e$ [7]. To see the emergence of the Porter-Thomas distribution, we write $\langle \mathbf{z} | \psi_M \rangle = a_{\mathbf{z}} + ib_{\mathbf{z}}$, where $a_{\mathbf{z}} = \sum_{\epsilon} d_{\epsilon}(\mathbf{z}) \cos \phi_{M,\epsilon}$ and $b_{\mathbf{z}} = \sum_{\epsilon} d_{\epsilon}(\mathbf{z}) \sin \phi_{M,\epsilon}$. Due to the Poisson distribution in the long time limit, the phases $\{\phi_{M,\epsilon}\}$ can be thought of as independent variables randomly and uni-

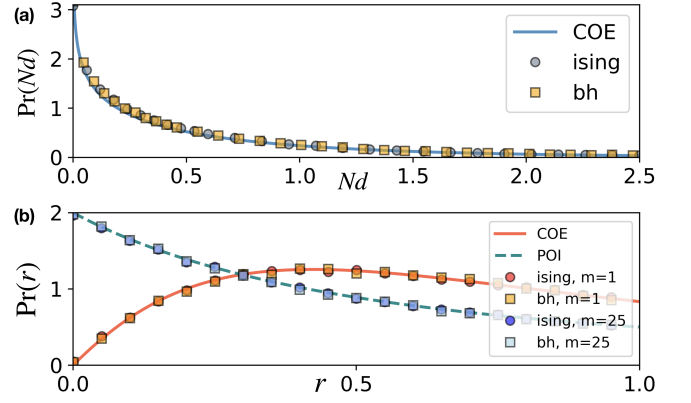


FIG. 2. (a) The eigenstate distribution $d_{\epsilon}(\mathbf{z})$ for the Ising and the Bose-Hubbard (BH) models. The blue line is the Bessel function of the second kind predicted by COE. (b) The statistics of level spacings obtained from the Ising and the Bose-Hubbard chain at $M = 1, 25$. The blue dashed and the solid lines are the POI and the COE distributions, respectively. Ising and Bose-Hubbard parameters: $L = 10$ (with half-filling for the BH model), $W = 1J, F = 2.5J, \omega = 8J$, and 500 disorder realizations.

l_1 -norm distance from Porter Thomas

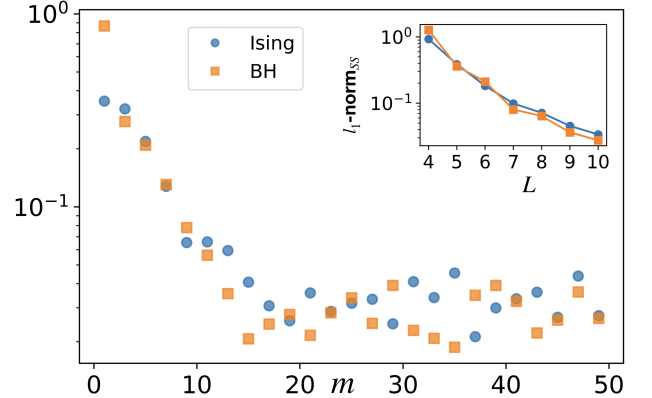


FIG. 3. The l_1 -norm distance between the output distribution from different quantum systems and the Porter-Thomas distribution at different m . The results from the Ising chain, the Bose-Hubbard chain, and random quantum circuits are labeled as crosses, squares, and circles, respectively. Ising and Bose-Hubbard parameters: $L = 10$ (with half-filling for the BH model), $W = 1J, F = 2.5J, \omega = 8J$, and 500 disorder realizations. The insert shows the plot of l_1 -norm distance in the long time limit as a function of L .

formly distributed in the range $[0, 2\pi)$. Using the product distribution formula and the central limit theorem, one can show that the distributions of $a_{\mathbf{z}}$ and $b_{\mathbf{z}}$ are normal distributions with zero mean and variance $1/2N$, see Methods. Since $p(\mathbf{z}) = a_{\mathbf{z}}^2 + b_{\mathbf{z}}^2$, the Porter-Thomas distribution of $p(\mathbf{z})$ can be derived using the fact that the square sum of Gaussian variables follows the χ -squared distribution with second degree of freedom [43].

Example of driven many-body models.- We give two

specific examples of driven systems that displays the COE statistics and, hence, partially supports Conjecture 2. For both cases, the modulation is $f(t) = \frac{1}{2}(1 - \cos(\omega t))$, where $\omega = 2\pi/T$ and initial states are randomized product states.

(i) 1D Ising model: We consider an Ising chain described by the Hamiltonian $\hat{H}_0^{\text{ISING}} = \sum_{l=0}^{L-1} \mu_l \hat{Z}_l + J \sum_{l=0}^{L-2} \hat{Z}_l \hat{Z}_{l+1}$, where $\mu_l \in \{0, W\}$ is a local disorder, W is the disorder strength, \hat{Z}_l is the Pauli's spin operator acting on site l , and J is the interaction strength. The drive is a global magnetic field $\hat{V}^{\text{ISING}} = F \sum_{l=0}^{L-1} \hat{X}_l$, where F is the driving amplitude. This simple model has been implemented in various quantum platforms, including Rydberg atoms [26], trapped ions [25] and superconducting circuits [27].

(ii) 1D Bose-Hubbard model: We consider the Bose-Hubbard model described by the Hamiltonian $\hat{H}_0^{\text{BM}} = \sum_{l=0}^{L-1} (\mu_l \hat{a}_l^\dagger \hat{a}_l + \frac{U}{2} \hat{a}_l^\dagger \hat{a}_l^\dagger \hat{a}_l \hat{a}_l)$, where \hat{a}_l is a bosonic annihilation operator at site l , U is the on-site interaction, and μ_l is the local disorder as defined above. The drive modulates the hopping amplitudes $\hat{V}^{\text{BH}} = -F \sum_{l=0}^{L-2} (\hat{a}_l^\dagger \hat{a}_{l+1} + H.c.)$. This model has been implemented in superconducting circuits [14] and cold atoms [28].

The distribution of $d_e(\mathbf{z})$ from both models are depicted in Fig. 2(a), showing an agreement with the Bessel function as predicted by COE. The level statistics at $M = 1$ and $M = 25$ are depicted in Fig. 2(b), showing an agreement with the COE and the POI distribution, respectively. The driving frequency and the disorder strength are tuned to ensure the observation of the thermalized phase and prevent many-body localization [31, 44].

Fig. 3 shows the l_1 -norm distance between $\text{Pr}(p)$ and the Porter-Thomas distribution at different m for the Ising and the Bose-Hubbard models. It can be seen that, in all cases, the system reaches the Porter-Thomas distribution after multiple driving cycles. The l_1 -norm distance in the long-time limit is decaying towards zero as the size of the system increased. Therefore, the anti-concentration condition is satisfied.

We note that analog quantum hardware has been shown experimentally to generate quantum dynamics beyond the reach of existing classical numerical methods. For example, in Ref. [20], cold atoms in optical lattices have been used to compute the quantum many-body localization transition in two-dimension. The transition cannot be efficiently computed by the state-of-the-art numerical technique such as tensor network [45]. However, such transition has not been shown theoretically to be hard to compute by a classical computer. Hence, quantum supremacy has yet to be achieved. Our work provides a theoretical foundation of the quantum supremacy for analog quantum simulators by showing the hardness of computing their output distribution.

III. CONCLUSIONS AND OUTLOOK

We have shown that, as long as ETH holds, periodically driven interacting quantum systems cannot be efficiently simulated on a classical computer. We provide analytical evidence of the computational hardness stemming from the COE statistics and provide numerical evidence for the COE dynamics obtained from the quantum Ising and the Bose-Hubbard chains, as expected from ETH. These two models serve as examples, among many, of physical analog quantum systems that follow the COE. Our results open up possibilities to realize quantum supremacy in a wide range of experimental platforms. In the future, it would be interesting to extend our results to a broader class of quantum many-body systems such as those with gauge fields, frustrated spin systems, and undriven systems.

IV. METHODS

A. A proof of Theorem 3

Let us consider a classical probabilistic computer with an NP oracle, also called a BPP^{NP} machine. This is a theoretical object that can solve problems in the third level of the polynomial hierarchy. The Stockmeyer theorem states that a BPP^{NP} machine with oracle access to a classical sampler \mathcal{C} , as defined in the main text, can efficiently output an approximation $\tilde{q}(\mathbf{z})$ of $q(\mathbf{z})$ such that

$$|q(\mathbf{z}) - \tilde{q}(\mathbf{z})| \leq \frac{q(\mathbf{z})}{\text{poly}(L)}. \quad (7)$$

The BPP^{NP} machine grants us the ability to perform the approximating task, in contrast to the machine \mathcal{C} that can only sample strings from a given distribution. To see how the BPP^{NP} machine can output a multiplicative approximation of $p_M(\mathbf{z})$ for most, but not all, $\mathbf{z} \in \mathcal{Z}$, let us consider

$$\begin{aligned} |p_M(\mathbf{z}) - \tilde{q}(\mathbf{z})| &\leq |p_M(\mathbf{z}) - q(\mathbf{z})| + |q(\mathbf{z}) - \tilde{q}(\mathbf{z})| \\ &\leq |p_M(\mathbf{z}) - q(\mathbf{z})| + \frac{q(\mathbf{z})}{\text{poly}(L)} \\ &\leq |p_M(\mathbf{z}) - q(\mathbf{z})| + \frac{|p_M(\mathbf{z}) - q(\mathbf{z})| + p_M(\mathbf{z})}{\text{poly}(L)} \\ &= \frac{p_M(\mathbf{z})}{\text{poly}(L)} + |p_M(\mathbf{z}) - q(\mathbf{z})| \left(1 + \frac{1}{\text{poly}(L)}\right). \end{aligned} \quad (8)$$

The first and the third lines are obtained using the triangular inequality. To get multiplicative approximation of $p_M(\mathbf{z})$ using $\tilde{q}(\mathbf{z})$, we need the term $|p_M(\mathbf{z}) - q(\mathbf{z})|$ to be small. Given the additive error defined in Eq. (3), this is indeed the case for a large portion of $\{\mathbf{z}\} \in \mathcal{Z}$; since the left hand side of Eq. (3) involves summing over an

exponentially large number of terms but the total error is bounded by a constant β , most of the terms in the sum must be exponentially small. This statement can be made precise using Markov's inequality.

Fact 1 (Markov's inequality) *If X is a nonnegative random variable and $a > 0$, then the probability that X is at least a is*

$$\Pr(X \geq a) \leq \frac{\mathbb{E}(X)}{a},$$

where $\mathbb{E}(X)$ is the expectation value of X .

By setting $X = |p_M(\mathbf{z}) - q(\mathbf{z})|$, we get

$$\Pr_{\mathbf{z}}(|p_M(\mathbf{z}) - q(\mathbf{z})| \geq a) \leq \frac{\mathbb{E}_{\mathbf{z}}(|p_M(\mathbf{z}) - q(\mathbf{z})|)}{a},$$

Here the distribution and the expectation value are computed over $\mathbf{z} \in \mathcal{Z}$. Note that $\mathbb{E}_{\mathbf{z}}(|p_M(\mathbf{z}) - q(\mathbf{z})|) \leq \beta/N$ is given by the additive error defined in Eq. (3). By setting $a = \beta/N\zeta$ for some small $\zeta > 0$, we get

$$\Pr_{\mathbf{z}}\left(|p_M(\mathbf{z}) - q(\mathbf{z})| \geq \frac{\beta}{N\zeta}\right) \leq \zeta$$

or equivalently

$$\Pr_{\mathbf{z}}\left(|p_M(\mathbf{z}) - q(\mathbf{z})| < \frac{\beta}{N\zeta}\right) > 1 - \zeta.$$

By substituting $|p_M(\mathbf{z}) - q(\mathbf{z})|$ from Eq. (8), we get

$$\Pr_{\mathbf{z}}\left(|p_M(\mathbf{z}) - \tilde{q}(\mathbf{z})| < \frac{p_M(\mathbf{z})}{\text{poly}(L)} + \frac{\beta}{N\zeta} \left(1 + \frac{1}{\text{poly}(L)}\right)\right) > 1 - \zeta. \quad (9)$$

From Theorem 2 (the anticoncentration condition), it follows that $1/N < p_M(\mathbf{z})$ for at least $1/e$ fraction of the unitary matrices in $\{\hat{U}_{\text{COE}}\}$. Hence, we can rewrite Eq. (9) as

$$\Pr_{\mathcal{Y}}\{|p_M(\mathbf{z}) - \tilde{q}(\mathbf{z})| < p_M(\mathbf{z}) \left[\frac{1}{\text{poly}(L)} + \frac{\beta}{\zeta} \left(1 + \frac{1}{\text{poly}(L)}\right) \right]\} > 1/e - \zeta. \quad (10)$$

Here, the distribution is over all $\mathbf{z} \in \mathcal{Z}$ and all unitary matrices in $\{\hat{U}_{\text{COE}}\}$, i.e. the set \mathcal{Y} as defined in Theorem 1. To understand the right hand side of the equation, let $P \cap Q$ be the intersection between the set P of probabilities that anticoncentrate and the set Q of probabilities that satisfy the Markov's inequality. Since $\Pr(P \cap Q) = \Pr(P) + \Pr(Q) - \Pr(P \cup Q) \geq \Pr(P) + \Pr(Q) - 1$, and $\Pr(P)$ and $\Pr(Q)$ are $1/e$ and $1 - \zeta$, respectively, it follows that $\Pr(P \cap Q)$ is no less than $1/e + 1 - \zeta - 1 = 1/e - \zeta$.

Following [38], we further set $\beta = 1/e$ and $\zeta = 1/4e$ so that

$$\Pr_{\hat{U}, \mathbf{z}}\left\{|p_M(\mathbf{z}) - \tilde{q}(\mathbf{z})| < \left(\frac{1}{4} + o(1)\right) p_M(\mathbf{z})\right\} > \frac{3}{4e}, \quad (11)$$

giving an approximation up to multiplicative error $1/4 + o(1)$ for at least $3/4e$ instances of the COE. Now since not all COE unitary matrices are realizable given a specific implementation of a periodically-driven unitary evolution, we subtract the success probability by $\eta = 1/4e$ in Conjecture 2. Thus, Stockmeyer algorithm is able to output a multiplicative approximation in the third level of the polynomial hierarchy for at least $1/2e$ fraction of $\{\hat{U}_F\}$. If, according to Conjecture 1, multiplicatively estimating $1/2e$ fraction of the probabilities is #P-hard, then the PH collapses and Theorem 3 is proved.

B. Mapping $p_M(\mathbf{z})$ to the partition function of a classical complex Ising model.

In this section, we prove Eq. (5) in the main text by providing justifications of the diagrammatic recipes to map the evolution \hat{U}_{CUE} on a Ising spin model with complex fields. The quantum gates of interest consist of both diagonal gates $\{T, CZ\}$ and non-diagonal gates $\{\sqrt{X}, \sqrt{Y}, \sqrt{Y}^T, H\}$. For simplicity, we start with one- and two- qubit examples before generalizing to the COE dynamics. The proof is adapted from Ref. [7].

1. One-qubit example

Let us consider a one-qubit circuit and $N + 1$ gates randomly chosen from the set $\{\sqrt{X}, \sqrt{Y}, \sqrt{Y}^T, T\}$. The zeroth gate is fixed to be a Hadamard gate. The output probability is $p(z) = |\langle z | \hat{U} | 0 \rangle|^2$, where $\hat{U} = \prod_{n=0}^N \hat{U}^{(n)}$ is the total unitary matrix, $\hat{U}^{(n)}$ is the n^{th} gate and $z \in \{0, 1\}$ is the readout bit. Below, we outline the mathematical steps underlying the diagrammatic approach followed by detailed explanations for each step:

$$p(z) = \left| \langle z | \prod_{n=0}^N \hat{U}^{(n)} | 0 \rangle \right|^2 \quad (12)$$

$$= \left| \sum_{\underline{z} \in \{0,1\}^N} \prod_{n=0}^N \langle z_n | \hat{U}^{(n)} | z_{n-1} \rangle \right|^2 \quad (13)$$

$$= \left| \sum_{\underline{z} \in \{0,1\}^N} \prod_{n=0}^N A(z_n, z_{n-1}) \exp \left[\frac{i\pi}{4} \Phi(z_n, z_{n-1}) \right] \right|^2 \quad (14)$$

$$= \left| \sum_{\underline{z} \in \{0,1\}^{N+2}} A(\underline{z}) \exp \left[\frac{i\pi}{4} \sum_{n=0}^N \Phi(z_n, z_{n-1}) \right] \right|^2. \quad (15)$$

$$(16)$$

In the second line, we inserted an identity $\hat{I}_n = \sum_{z_n \in \{0,1\}} |z_n\rangle \langle z_n|$ between $\hat{U}^{(n+1)}$ and $\hat{U}^{(n)}$ for every

$n \in \{0, \dots, N-1\}$. This line can be interpreted as the Feynman's path integral where each individual path or 'world-line' is characterized by a sequence of basis variables $\underline{z} = (z_{-1}, z_0, \dots, z_N)$. The initial and the end points for every path are $|z_{-1}\rangle = |0\rangle$ and $|z_N\rangle = |z\rangle$, respectively. In the third line, we decompose $\langle z_n | \tilde{U}^{(n)} | z_{n-1} \rangle$ into the amplitude $A(z_n, z_{n-1})$ and phase $\Phi(z_n, z_{n-1})$. In the fourth line, we introduce $A(\underline{z}) = \prod_{n=0}^N A(z_n, z_{n-1})$. The equation now takes the form of the partition of a classical Ising model with complex energies. Here, \underline{z} can be interpreted as a classical spin configuration, $A(\underline{z})$ as the degeneracy number and $i\frac{\pi}{4}\Phi(z_n, z_{n-1})$ as a complex energy associated with spin-spin interaction.

Further simplifications are possible by noting that, the diagonal gates in the circuits allow the reduction of the number of classical spins. Specifically, if a T gate is applied to $|z_{n-1}\rangle$, it follows that $z_n = z_{n-1}$. Hence, the variables z_{n-1} and z_n can be represented by a single classical spin state. The two variables z_{n-1}, z_n become independent only when a non-diagonal gate is applied. Therefore, we can group all variables $\{z_n\}$ between two non-diagonal gates as one classical spin. This procedure leads to the directives presented as the STEP I of the procedure in the main text. Formally, for $N_{\text{spin}} + 1$ non-diagonal gates in the circuit (including the first Hadamard gate) \underline{z} can be characterized by a classical spin configuration $\underline{s} = (s_{-1}, s_0, \dots, s_k, \dots, s_{N_{\text{spin}}})$ where $s_k = 1 - 2z_k \in \{\pm 1\}$ is a spin representing the basis variable immediately after the k^{th} non-diagonal gate, i.e.

$$\sqrt{X} = \frac{1}{\sqrt{2}} \begin{pmatrix} e^{\frac{i\pi}{2}} & 1 \\ 1 & e^{\frac{i\pi}{2}} \end{pmatrix} = \frac{1}{\sqrt{2}} \left[e^{\frac{i\pi}{4}(1+s_k s_{k-1})} \right]_{s_k, s_{k-1}}, \quad (20)$$

$$\sqrt{Y} = \frac{1}{\sqrt{2}} \begin{pmatrix} 1 & -1 \\ 1 & 1 \end{pmatrix} = \frac{1}{\sqrt{2}} \left[e^{\frac{i\pi}{4}(1-s_{k-1})(1+s_k)} \right]_{s_k, s_{k-1}}, \quad (21)$$

$$\sqrt{Y}^T = \frac{1}{\sqrt{2}} \begin{pmatrix} 1 & 1 \\ -1 & 1 \end{pmatrix} = \frac{1}{\sqrt{2}} \left[e^{\frac{i\pi}{4}(1+s_{k-1})(1-s_k)} \right]_{s_k, s_{k-1}}, \quad (22)$$

$$H = \frac{1}{\sqrt{2}} \begin{pmatrix} 1 & 1 \\ 1 & -1 \end{pmatrix} = \frac{1}{\sqrt{2}} \left[e^{\frac{i\pi}{4}(1-s_{k-1})(1-s_k)} \right]_{s_k, s_{k-1}}, \quad (23)$$

$$T = \begin{pmatrix} 1 & 0 \\ 0 & e^{\frac{i\pi}{4}} \end{pmatrix} = \text{Diag} \left[e^{\frac{i\pi}{4}(\frac{1-s_k}{2})} \right]_{s_k} \quad (24)$$

Notice that all non-diagonal gates contribute to the same amplitude $A(s_k, s_{k-1}) = 1/\sqrt{2}$, leading to $A(\underline{s}) = 2^{-(N_{\text{spin}}+1)/2}$. Hence, we can extract the contribution of each gate to $\Phi(s_k, s_{k-1})$ as

$$\Phi_{\sqrt{X}}(s_k, s_{k-1}) = 1 + s_{k-1}s_k, \quad (25)$$

$$\Phi_{\sqrt{Y}}(s_k, s_{k-1}) = (1 - s_{k-1})(1 + s_k) \quad (26)$$

$$= 1 - s_{k-1} + s_k - s_{k-1}s_k, \quad (27)$$

$$\Phi_{\sqrt{Y}^T}(s_k, s_{k-1}) = (1 + s_{k-1})(1 - s_k) \quad (28)$$

$$= 1 + s_{k-1} - s_k - s_{k-1}s_k, \quad (29)$$

$$\Phi_T(s_k) = \frac{1 - s_k}{2}. \quad (30)$$

The under-script indicates which gate is contributing to the phase. The corresponding h_i , h_j and J_{ij} are depicted in the lookup table in Fig. 1(f) in the main text, where $i = k-1$ and $j = k$. The global phase that does not depend on \underline{s} is ignored as it does not contribute to $p(z)$.

2. Two-qubit example

Now we consider a two-qubit random circuits to demonstrate the action of the CZ gates. We introduce a new index $l \in \{1, 2\}$ to label each qubit, which is placed on a given horizontal line (row). Since the CZ gate is diagonal, its presence does not alter the number of spins in each row. However, the gate introduces interaction between spins in different rows. This can be seen from its explicit form, i.e.

$$CZ = \begin{pmatrix} 1 & 0 & 0 & 0 \\ 0 & 1 & 0 & 0 \\ 0 & 0 & 1 & 0 \\ 0 & 0 & 0 & -1 \end{pmatrix} = \text{Diag} \left[e^{\frac{i\pi}{4}(1-s_{1,k})(1-s_{2,k'})} \right]_{s_{1,k}, s_{2,k'}}, \quad (31)$$

Lastly, we need to specify $A(\underline{s})$ and $\Phi(s_k, s_{k-1})$ in term of the local fields h_{k-1} , h_k , the interaction $J_{k-1,k}$, and spin configurations s_{k-1}, s_k . This is done by writing the gates in their matrix form, i.e.

where $s_{1,k}$ ($s_{2,k'}$) is the state of the k^{th} (k'^{th}) spin at the first (second) row. It follows that

$$\Phi_{s_{1,k},s_{2,k'}}^{CZ} = (1 - s_{1,k})(1 - s_{2,k'}) \quad (32)$$

$$= 1 - s_{1,k} - s_{2,k'} + s_{1,k}s_{2,k'}. \quad (33)$$

The corresponding h_i , h_j , and J_{ij} are depicted in Fig. 1(f) in the maintext, where $i = (1, k)$ and $j = (2, k')$. We have now derived all necessary ingredients to map a random quantum circuit to a classical Ising model.

3. Full COE dynamics

Since the COE dynamics can be expressed in terms of a quasi-random quantum circuit, we can straightforwardly apply the above procedure to find the corresponding Ising model. The complexity here solely arises from the number of indices required to specify the positions of all the gates in the circuit. To deal with this, we introduce the following indices

- an index $l \in \{1, \dots, L\}$ to indicate which qubit / row.
- an index $m \in \{1, \dots, M\}$ to indicate which period.
- an index $\mu \in \{A, B\}$ to indicate which part of the period. A and B refer to the \hat{U}_{CUE} part and the \hat{U}_{CUE}^T part, respectively
- an index $k \in \{0, 1, \dots, N_{\text{spin}}(l)\}$ to indicate the spin position for a given m and μ . Here, $N_{\text{spin}}(l)$ is the total number of spins at the l^{th} row. Note that due to the symmetric structure of \hat{U}_{CUE} and \hat{U}_{CUE}^T , we run the index k backward for the transpose part, i.e. $k = 0$ refers to the last layer.
- an index $\nu_{l,k}$ so that $\nu_{l,k} = 1$ if the k^{th} non-diagonal gate acting on the qubit l is \sqrt{X} otherwise $\nu_{l,k} = 0$.

With these indices, the partition function of the circuit, as shown in Fig. 1(a), can be written as

$$\langle \mathbf{z} | \psi \rangle = 2^{-\frac{G}{2}} \sum_{\underline{s} \in \mathcal{S}} \exp \left[\frac{i\pi}{4} E(\underline{s}) \right], \quad (34)$$

with

$$E(\underline{s}) = \sum_{m=1}^M \sum_{\mu=A}^B \sum_{l=1}^L \sum_{k=0}^{N_{\text{spin}}(l)} h_{lk} s_{l,k}^{\mu,m} \quad (35)$$

$$+ \sum_{m=1}^M \sum_{\mu=A}^B \sum_{l=1}^L \sum_{k=1}^{N_{\text{spin}}(l)} (2\nu_{l,k} - 1) s_{l,k-1}^{\mu,m} s_{l,k}^{\mu,m} \quad (36)$$

$$+ \sum_{m=1}^M \sum_{\mu=A}^B \sum_{l=1}^L \sum_{l'=1}^{l-1} \sum_{k=1}^{N_{\text{spin}}(l)} \sum_{k'=1}^{N_{\text{spin}}(l')} \zeta_{(l,k)}^{(l',k')} s_{l,k}^{\mu,m} s_{l',k'}^{\mu,m} \quad (37)$$

$$+ E(\mathbf{z}), \quad (38)$$

$$h_{lk} = \nu_{l,k+1} - \nu_{l,k} - \frac{1}{2} N_T(l, k) - N_{CZ}(l, k), \quad (39)$$

$$E(\mathbf{z}) = -s_{0,l}^{B,M} - s_{z_l} + s_{0,l}^{B,M} s_{z_l}, \quad (40)$$

where G is the total number of non-diagonal gates in the circuit. $\zeta_{(l,k)}^{(l',k')}$ represents the total number of CZ gates which introduces the interaction between spins $s_{l,k}^{\mu,m}$ and $s_{l',k'}^{\mu,m}$. $N_{CZ}(l, k)$ ($N_T(l, k)$) is the total number of CZ (T) gates which introduces local fields on the spin $s_{l,k}^{\mu,m}$. $E(\mathbf{z})$ is the contribution from the last Hadamard layer which depends on the readout bit-string \mathbf{z} . $\{s_{z_l}\}$ are the spins corresponding to \mathbf{z} and their configuration is fixed. In addition, there are also two extra boundary conditions (i) between part A and B and (ii) between the two adjacent periods m and $m+1$, i.e. $s_{l, N_{\text{spin}}(l)}^{A,m} = s_{l, N_{\text{spin}}(l)}^{B,m}$ and $s_{l,0}^{A,m+1} = s_{l,0}^{B,m}$.

C. Derivation of Porter-Thomas distribution from COE dynamics.

In this section, we show that the distribution of the output probability of COE dynamics, $\text{Pr}(p)$, follows the Porter-Thomas distribution $\text{Pr}_{\text{PT}}(p) = N e^{-Np}$. Let us consider the output probability $p_M(\mathbf{z}) = |\langle \mathbf{z} | \psi_M \rangle|^2$ with

$$\langle \mathbf{z} | \psi_M \rangle = \langle \mathbf{z} | U_{\text{COE}}^M | \mathbf{0} \rangle \quad (41)$$

$$= \langle \mathbf{z} | \left[\sum_{\epsilon=0}^{N-1} e^{iME_{\epsilon}T} |E_{\epsilon}\rangle \langle E_{\epsilon}| \right] | \mathbf{0} \rangle \quad (42)$$

$$= \sum_{\epsilon=0}^{N-1} d_{\epsilon}(\mathbf{z}) e^{i\phi_{M,\epsilon}} \quad (43)$$

$$= \left[\sum_{\epsilon=0}^{N-1} d_{\epsilon}(\mathbf{z}) \cos \phi_{M,\epsilon} \right] + i \left[\sum_{\epsilon=0}^{N-1} d_{\epsilon}(\mathbf{z}) \sin \phi_{M,\epsilon} \right] \quad (44)$$

$$= a_{\mathbf{z}} + ib_{\mathbf{z}}, \quad (45)$$

where N is the dimension of the Hilbert space, $d_{\epsilon}(\mathbf{z}) = \langle \mathbf{z} | E_{\epsilon} \rangle \langle E_{\epsilon} | \mathbf{0} \rangle$, $\phi_{m,\epsilon} = ME_{\epsilon}T \bmod 2\pi$, $a_{\mathbf{z}} = \text{Re}[\langle \mathbf{z} | \psi_M \rangle]$ and $b_{\mathbf{z}} = \text{Im}[\langle \mathbf{z} | \psi_M \rangle]$. Below, we will prove the following theorems.

Theorem 4 The distribution of $d_\epsilon(\mathbf{z})$ over $\forall \epsilon \in \{0, \dots, N-1\}$ or $\forall \mathbf{z} \in \{0, 1\}^L$ is the Bessel function of the second kind.

Theorem 5 The distribution of $a_{\mathbf{z}}$ and $b_{\mathbf{z}}$ over $\forall \mathbf{z} \in \{0, 1\}^L$ is the normal distribution with zero mean and variance $1/2N$.

Theorem 6 The distribution of $a_{\mathbf{z}}^2 + b_{\mathbf{z}}^2$ over $\forall \mathbf{z} \in \{0, 1\}^L$ is the Porter-Thomas distribution, Pr_{PT} .

To prove Theorem 4, we first write $d_\epsilon(\mathbf{z}) = c_{\mathbf{z},\epsilon} c_{0,\epsilon}$, where $c_{\mathbf{z},\epsilon} = \langle \mathbf{z} | E_\epsilon \rangle$ and $c_{0,\epsilon} = \langle \mathbf{0} | E_\epsilon \rangle$. For the COE dynamics, the coefficients $c_{\mathbf{z},\epsilon}$ and $c_{0,\epsilon}$ are real numbers whose distribution is [39]

$$\text{Pr}(c) = \sqrt{\frac{2N}{\pi}} \exp\left[-\frac{Nc^2}{2}\right]. \quad (46)$$

As discussed in the main text, the phase $\phi_{M,\epsilon}$ becomes random as $M \gg 2\pi/E_\epsilon T$. The random sign (± 1) from $c_{\mathbf{z},\epsilon}$ can therefore be absorbed into the phase without changing its statistics. The distribution of $d_\epsilon(\mathbf{z})$ can be obtained using the product distribution formula

$$\text{Pr}(d) = \int_0^\infty \text{Pr}(c) \text{Pr}\left(\frac{d}{c}\right) \cdot \frac{1}{c} \cdot dc \quad (47)$$

$$= \frac{2N}{\pi} \int_0^\infty \exp\left(-\frac{Nc^2}{2}\right) \exp\left(-\frac{Nd^2}{2c^2}\right) dc \quad (48)$$

$$= \frac{2N}{\pi} K_0(Nd), \quad (49)$$

where K_0 is the modified Bessel function of the second kind.

To prove Theorem 5, we first note that the distribution of $\cos \phi_{m,\epsilon}$ and $\sin \phi_{m,\epsilon}$ are

$$\text{Pr}(\cos \phi) = \frac{1}{\pi \sqrt{1 - \cos^2 \phi}}, \quad (50)$$

$$\text{Pr}(\sin \phi) = \frac{1}{\pi \sqrt{1 - \sin^2 \phi}}. \quad (51)$$

Here, we have used the fact that $\phi_{M,\epsilon}$ is uniformly distributed in the range $[0, 2\pi)$. We then calculate the distribution of $\kappa_\epsilon \equiv d_\epsilon(\mathbf{z}) \cos \phi_{M,\epsilon}$ using the product distribution formula, i.e.

$$\text{Pr}(\kappa) = \int_{-1}^1 \frac{1}{\pi \sqrt{1 - \cos^2 \phi}} \cdot \frac{2N}{\pi} K_0\left(\frac{N\kappa}{d}\right) \cdot \frac{1}{\cos \phi} d \cos \phi \quad (52)$$

$$= \frac{N}{\pi^2} K_0^2\left(\frac{N|\kappa|}{2}\right). \quad (53)$$

The mean and the variance of κ_ϵ can be calculated as

$$\langle \kappa \rangle = \int_{-\infty}^{\infty} d \cos \phi \cdot \frac{N}{\pi^2} \cdot K_0^2\left(\frac{N|\kappa|}{2}\right) \cdot d\kappa = 0 \quad (54)$$

$$\text{Var}(\kappa) = \int_{-\infty}^{\infty} (d \cos \phi)^2 \cdot \frac{N}{\pi^2} \cdot K_0^2\left(\frac{N|\kappa|}{2}\right) \cdot d\kappa = \frac{1}{2N^2}. \quad (55)$$

Since $a_{\mathbf{z}}$ is a sum of independent and identically distributed random variables, i.e. $a_{\mathbf{z}} = \sum_{\epsilon=1}^{N-1} \kappa_\epsilon$, we can apply the central limit theorem for large N . Hence, the distribution of $a_{\mathbf{z}}$ is normal with the mean zero and variance $\text{Var}(a) = N\text{Var}(\kappa) = 1/2N$. The same applies for the distribution of $b_{\mathbf{z}}$.

Theorem 6 can be proven using the fact that the square sum of the Gaussian variable follows the χ -squared distribution with second degree of freedom $\text{Pr}_{\chi^2, k=2}(p) \sim \exp\{-p/2\sigma^2\}$ [43]. By specifying the variance obtained in Theorem 5 and normalization, we arrive at the desired Porter-Thomas distribution.

V. ACKNOWLEDGEMENT

This research is supported by the National Research Foundation, Prime Minister's Office, Singapore and the Ministry of Education, Singapore under the Research Centres of Excellence programme. It was also partially funded by Polisimulator project co-financed by Greece and the EU Regional Development Fund, the European Research Council under the European Union's Seventh Framework Programme (FP7/2007-2013)/ Ninnat Dangiannam is supported by the National Natural Science Foundation of China (Grant No. 11875110).

VI. COMPETING INTERESTS

The authors declare that there are no competing interests.

VII. AUTHOR CONTRIBUTION

J.T. and S.T. performed numerical simulations. M.A.L., N. D. and D.G.A provided theoretical assistance. All five authors contributed to writing the paper.

VIII. DATA AVAILABILITY

The data that support the findings of this study are available from the corresponding author upon reasonable request.

-
- [1] John Preskill. Quantum Computing in the NISQ era and beyond. *Quantum*, 2:79, August 2018.
- [2] A. W. Harrow and A. Montanaro. Quantum computational supremacy. *Nature*, 549:203, 09 2017.
- [3] S. Aaronson and A. Arkhipov. The computational complexity of linear optics. *Proceedings of the 43rd annual ACM Symposium on Theory of Computing, (STOC '11)*, pages 333–342, 2011.
- [4] Aaronson Scott. A linear-optical proof that the permanent is np-hard. *Proceedings of the Royal Society A: Mathematical, Physical and Engineering Sciences*, 467:3393, 2011.
- [5] A. P. Lund, Michael J. Bremner, and T. C. Ralph. Quantum sampling problems, bosonsampling and quantum supremacy. *npj Quantum Information*, 3(1):15, 2017.
- [6] Michael J. Bremner, Richard Jozsa, and Dan J. Shepherd. Classical simulation of commuting quantum computations implies collapse of the polynomial hierarchy. *Proceedings of the Royal Society A: Mathematical, Physical and Engineering Sciences*, 467(2126):459–472, 2011.
- [7] S. Boixo, S. V. Isakov, V. N. Smelyanskiy, R. Babbush, N. Ding, Z. Jiang, M. J. Bremner, J. M. Martinis, and H. Neven. Characterizing quantum supremacy in near-term devices. *Nature Physics*, 14(6):595–600, 2018.
- [8] Adam Bouland, Bill Fefferman, Chinmay Nirkhe, and Umesh Vazirani. On the complexity and verification of quantum random circuit sampling. *Nature Physics*, 15(2):159–163, 2019.
- [9] J. B. Spring, B. J. Metcalf, P. C. Humphreys, W. S. Kolthammer, X.-M. Jin, M. Barbieri, A. Datta, N. Thomas-Peter, N. K. Langford, D. Kundys, J. C. Gates, B. J. Smith, P. G. R. Smith, and I. A. Walsley. Boson sampling on a photonic chip. *Science*, 339(6121):798–801, 2013.
- [10] M. A. Broome, A. Fedrizzi, S. Rahimi-Keshari, J. Dove, S. Aaronson, T. C. Ralph, and A. G. White. Photonic boson sampling in a tunable circuit. *Science*, 339(6121):794–798, 2013.
- [11] M. Tillmann, B. Dakić, R. Heilmann, S. Nolte, A. Szameit, and P. Walther. Experimental boson sampling. *Nature Photonics*, 7:540, 05 2013.
- [12] A. Crespi, R. Osellame, R. Ramponi, D. J. Brod, E. F. Galvão, N. Spagnolo, C. Vitelli, E. Maiorino, P. Mataloni, and F. Sciarrino. Integrated multimode interferometers with arbitrary designs for photonic boson sampling. *Nature Photonics*, 7:545, 05 2013.
- [13] Hui Wang, Jian Qin, Xing Ding, Ming-Cheng Chen, Si Chen, Xiang You, Yu-Ming He, Xiao Jiang, L. You, Z. Wang, C. Schneider, Jelmer J. Renema, Sven Höfling, Chao-Yang Lu, and Jian-Wei Pan. Boson sampling with 20 input photons and a 60-mode interferometer in a 10^{14} -dimensional hilbert space. *Phys. Rev. Lett.*, 123:250503, Dec 2019.
- [14] C. Neill, P. Roushan, K. Kechedzhi, S. Boixo, S. V. Isakov, V. Smelyanskiy, A. Megrant, B. Chiaro, A. Dunsworth, K. Arya, R. Barends, B. Burkett, Y. Chen, Z. Chen, A. Fowler, B. Foxen, M. Giustina, R. Graff, E. Jeffrey, T. Huang, J. Kelly, P. Klimov, E. Lucero, J. Mutus, M. Neeley, C. Quintana, D. Sank, A. Vainsencher, J. Wenner, T. C. White, H. Neven, and J. M. Martinis. A blueprint for demonstrating quantum supremacy with superconducting qubits. *Science*, 360(6385):195–199, 2018.
- [15] Frank Arute, Kunal Arya, Ryan Babbush, Dave Bacon, Joseph C. Bardin, Rami Barends, Rupak Biswas, Sergio Boixo, Fernando G. S. L. Brandao, David A. Buell, Brian Burkett, Yu Chen, Zijun Chen, Ben Chiaro, Roberto Collins, William Courtney, Andrew Dunsworth, Edward Farhi, Brooks Foxen, Austin Fowler, Craig Gidney, Marissa Giustina, Rob Graff, Keith Guerin, Steve Habegger, Matthew P. Harrigan, Michael J. Hartmann, Alan Ho, Markus Hoffmann, Trent Huang, Travis S. Humble, Sergei V. Isakov, Evan Jeffrey, Zhang Jiang, Dvir Kafri, Kostyantyn Kechedzhi, Julian Kelly, Paul V. Klimov, Sergey Knysh, Alexander Korotkov, Fedor Kostritsa, David Landhuis, Mike Lindmark, Erik Lucero, Dmitry Lyakh, Salvatore Mandrà, Jarrod R. McClean, Matthew McEwen, Anthony Megrant, Xiao Mi, Kristel Michielsen, Masoud Mohseni, Josh Mutus, Ofer Naaman, Matthew Neeley, Charles Neill, Murphy Yuezhen Niu, Eric Ostby, Andre Petukhov, John C. Platt, Chris Quintana, Eleanor G. Rieffel, Pedram Roushan, Nicholas C. Rubin, Daniel Sank, Kevin J. Satzinger, Vadim Smelyanskiy, Kevin J. Sung, Matthew D. Trevithick, Amit Vainsencher, Benjamin Villalonga, Theodore White, Z. Jamie Yao, Ping Yeh, Adam Zalcman, Hartmut Neven, and John M. Martinis. Quantum supremacy using a programmable superconducting processor. *Nature*, 574(7779):505–510, 2019.
- [16] J. I. Cirac and P. Zoller. Goals and opportunities in quantum simulation. *Nat Phys*, 8:264, 04 2012.
- [17] P. Hauke, F. M. Cucchietti, L. Tagliacozzo, I. Deutsch, and M. Lewenstein. Can one trust quantum simulators? *Reports on Progress in Physics*, 75(8):082401, 2012.
- [18] T. H. Johnson, S. R. Clark, and D. Jaksch. What is a quantum simulator? *EPJ Quantum Technology*, 1(1):10, Jul 2014.
- [19] I. M. Georgescu, S. Ashhab, and Franco Nori. Quantum simulation. *Rev. Mod. Phys.*, 86:153–185, Mar 2014.
- [20] J.-Y. Choi, S. Hild, J. Zeiher, P. Schauß, A. Rubio-Abadal, T. Yefsah, V. Khemani, D. A. Huse, I. Bloch, and C. Gross. Exploring the many-body localization transition in two dimensions. *Science*, 352(6293):1547–1552, 2016.
- [21] Juan Bermejo-Vega, Dominik Hangleiter, Martin Schwarz, Robert Raussendorf, and Jens Eisert. Architectures for quantum simulation showing a quantum speedup. *Phys. Rev. X*, 8:021010, Apr 2018.
- [22] Xun Gao, Sheng-Tao Wang, and L.-M. Duan. Quantum supremacy for simulating a translation-invariant ising spin model. *Phys. Rev. Lett.*, 118:040502, Jan 2017.
- [23] Leonardo Novo, Juani Bermejo-Vega, and Raúl García-Patrón. Quantum advantage from energy measurements of many-body quantum systems. *arXiv e-prints*, page arXiv:1912.06608, Dec 2019.
- [24] Pranjal Bordia, Henrik Lüschen, Ulrich Schneider, Michael Knap, and Immanuel Bloch. Periodically driving a many-body localized quantum system. *Nature Physics*, 13:460 EP –, 01 2017.
- [25] J. Zhang, G. Pagano, P. W. Hess, A. Kyprianidis, P. Becker, H. Kaplan, A. V. Gorshkov, Z. X. Gong, and C. Monroe. Observation of a many-body dynami-

- cal phase transition with a 53-qubit quantum simulator. *Nature*, 551:601, 11 2017.
- [26] H. Bernien, S. Schwartz, A. Keesling, H. Levine, A. Omran, H. Pichler, S. Choi, A. S. Zibrov, M. Endres, M. Greiner, V. Vuletić, and M. D. Lukin. Probing many-body dynamics on a 51-atom quantum simulator. *Nature*, 551:579, 11 2017.
- [27] J. S. Otterbach, R. Manenti, N. Alidoust, A. Bestwick, M. Block, B. Bloom, S. Caldwell, N. Didier, E. Schuyler Fried, S. Hong, P. Karalekas, C. B. Osborn, A. Papa-george, E. C. Peterson, G. Prawiroatmodjo, N. Rubin, Colm A. Ryan, D. Scarabelli, M. Scheer, E. A. Sete, P. Sivarajah, Robert S. Smith, A. Staley, N. Tezak, W. J. Zeng, A. Hudson, Blake R. Johnson, M. Reagor, M. P. da Silva, and C. Rigetti. Unsupervised Machine Learning on a Hybrid Quantum Computer.
- [28] Antonio Rubio-Abadal, Matteo Ippoliti, Simon Hollerith, David Wei, Jun Rui, S. L. Sondhi, Vedika Khemani, Christian Gross, and Immanuel Bloch. Floquet prethermalization in a Bose-Hubbard system. *arXiv e-prints*, page arXiv:2001.08226, Jan 2020.
- [29] J. Eisert, Friesdorf M., and C. Gogolin. Quantum many-body systems out of equilibrium. *Nature Physics*, (11):124–130, 2015.
- [30] L. D’Alessio, Y. Kafri, A. Polkovnikov, and M. Rigol. From quantum chaos and eigenstate thermalization to statistical mechanics and thermodynamics. *Advances in Physics*, 65(3):239–362, 2016.
- [31] L. D’Alessio and M. Rigol. Long-time behavior of isolated periodically driven interacting lattice systems. *Phys. Rev. X*, 4:041048, Dec 2014.
- [32] Jens Eisert, Dominik Hangleiter, Nathan Walk, Ingo Roth, Damian Markham, Rhea Parekh, Ulysse Chabaud, and Elham Kashefi. Quantum certification and benchmarking. *Nature Reviews Physics*, 2(7):382–390, 2020.
- [33] Dominik Hangleiter, Juan Bermejo-Vega, Martin Schwarz, and Jens Eisert. Anticoncentration theorems for schemes showing a quantum speedup. *Quantum*, 2:65, May 2018.
- [34] Larry. Stockmeyer. On approximation algorithms for $\#P$. *SIAM Journal on Computing*, 14(4):849–861, 1985.
- [35] $f(n) = o(g(n))$ means that $f(n)/g(n) \rightarrow 0$ when $n \rightarrow \infty$.
- [36] Even though there are recent breakthrough worst-to-average case reduction for hardness of computing output probabilities of quantum circuits. So far none of the approaches matches the realistic error requirement to rule out a classical sampler from the Stockmeyer argument [46, 47].
- [37] Leslie Ann Goldberg and Heng Guo. The complexity of approximating complex-valued ising and tutte partition functions. *computational complexity*, 26(4):765833, 2017.
- [38] Michael J. Bremner, Ashley Montanaro, and Dan J. Shepherd. Average-Case Complexity Versus Approximate Simulation of Commuting Quantum Computations. *Phys. Rev. Lett.*, 117(8):080501, August 2016. Publisher: American Physical Society.
- [39] Fritz Haake. *Quantum Signatures of Chaos*. Springer International Publishing, US, 2010.
- [40] Daniel A. Roberts and Beni Yoshida. Chaos and complexity by design. *Journal of High Energy Physics*, 2017(4):121, 2017.
- [41] Aram W. Harrow and Richard A. Low. Random quantum circuits are approximate 2-designs. *Communications in Mathematical Physics*, 291(1):257–302, Oct 2009.
- [42] Nicholas R. Jones. Chaos and randomness in strongly-interacting quantum systems. *Dissertation (Ph.D.)*, California Institute of Technology., 2018.
- [43] Marvin K. Simon. *Probability Distributions Involving Gaussian Random Variables*. Springer, Boston, MA, 2002.
- [44] Jirawat Tangpanitanon, Supanut Thanasilp, Marc-Antoine Lemonde, and Dimitris G. Angelakis. Quantum supremacy with analog quantum processors for material science and machine learning. *arXiv e-prints*, page arXiv:1906.03860, Jun 2019.
- [45] F. Verstraete, V. Murg, and J.I. Cirac. Matrix product states, projected entangled pair states, and variational renormalization group methods for quantum spin systems. *Advances in Physics*, 57(2):143–224, 2008.
- [46] Adam Bouland, Bill Fefferman, Chinmay Nirkhe, and Umesh Vazirani. On the complexity and verification of quantum random circuit sampling. *Nature Physics*, 15(2):159–163, 2019.
- [47] Ramis Movassagh. Cayley path and quantum computational supremacy: A proof of average-case $\#P$ -hardness of Random Circuit Sampling with quantified robustness. *arXiv:1909.06210 [cond-mat, physics:hep-th, physics:math-ph, physics:quant-ph]*, October 2019. arXiv:1909.06210.